High-resolution infrared absorption spectra, crystal-field levels, and relaxation processes in $CsCdBr_3:Pr^{3+}$

M. N. Popova and E. P. Chukalina
Institute of Spectroscopy, Russian Academy of Sciences, 142190 Troitsk, Moscow Region, Russia

B. Z. Malkin and A. I. Iskhakova
Kazan State University, 420008 Kazan, Russia

E. Antic-Fidancev and P. Porcher
CNRS-UMR 7574 ENSCP, Laboratoire de Chimie Appliquee de l'Etat Solide, 11, Rue P. et M. Curie, 75231 Paris Cedex 05, France

J. P. Chaminade
Institut de Chimie de la Matière Condensée de Bordeaux, ICMCB–CNRS, Château Brivazac, Avenue du Docteur Schweitzer, F-33608 Pessac Cedex, France

(Received 15 June 1999; published 22 January 2001)

High-resolution low-temperature absorption spectra of 0.2% Pr^{3+}-doped $CsCdBr_3$ were measured in the spectral region 2000–7000 cm^{-1}. Positions and widths of the crystal-field levels within the $^3H_5$, $^3H_4$, $^3F_2$, and $^3F_3$ multiplets of the Pr^{3+} main center have been determined. The hyperfine structure of several spectral lines has been found. Crystal-field calculations were carried out in the framework of the semiphenomenological exchange charge model (ECM). Parameters of the ECM were determined by fitting to the measured total splittings of the $^3H_4$ and $^3H_6$ multiplets and to the observed hyperfine splittings of the crystal-field levels in this work. One- and two-phonon relaxation rates were calculated using the phonon Green's functions of the perfect ($CsCdBr_3$) and locally perturbed (impurity dimer centers in $CsCdBr_3:Pr^{3+}$) crystal lattice. Comparison with the measured linewidths confirmed an essential redistribution of the phonon density of states in $CsCdBr_3$ crystals doped with rare-earth ions.

DOI: 10.1103/PhysRevB.63.075103 PACS number(s): 78.55.Fv, 78.30.Hv

I. INTRODUCTION

Crystals of rare-earth (R) doped quasi-one-dimensional double bromides $CsCdBr_3$ are widely studied, mainly because of their property to incorporate R^{3+} ions in pairs, even at low R concentrations. This makes them a promising material for up-conversion lasers. The structure of $CsCdBr_3$ belongs to the D_{6h}^4 space group and consists of linear chains of face-sharing $[CdBr_6]^{4-}$ octahedra along the c axis. The positional symmetry for Cd^{2+} is D_{3d}. R^{3+} ions substitute for Cd^{2+}, forming centers with different mechanisms of charge compensation. The main center consists of two R^{3+} ions placed in the chain on each side of an adjacent cadmium vacancy, $[R^{3+}–Cd^{2+}$ vacancy$–R^{3+}]$.[1–3] Both R^{3+} ions in such a center are equivalent; their positional symmetry lowers from D_{3d} to C_{3v}. Spectra of many other centers with different configurations were reported in EPR and optical studies of $CsCdBr_3:R^{3+}$ crystals. In particular, positional symmetry for R^{3+} ions in minor axial centers that are supposed to appear at higher R concentrations, namely, $[R^{3+}–R^{3+}–Cd^{2+}$ vacancy$]$ or $[R^{3+}–Cd^{2+}$ vacancy$–Cd^{2+}–R^{3+}]$, is again C_{3v} but two R^{3+} positions are not equivalent, while in $[R^{3+}–Cs^{+}$ vacancy$]$ centers the positional symmetry of the R^{3+} ion is C_s.

Though the spectra of $CsCdBr_3:Pr^{3+}$ were intensively studied before,[1–5] crystal-field energies of the lowest excited multiplets were not investigated in absorption. The positions of crystal-field levels for the main center, as reported by different authors, differ by 2–14 cm^{-1}. The typical spectral resolution used in the mentioned works was 0.8–2 cm^{-1}, while the only high-resolution study (which concerned the $^1D_2$ level) revealed spectral lines as narrow as 0.1 cm^{-1}.[1,5] A peculiar doublet line shape was observed for the $^3H_4(\Gamma_1) \rightarrow {}^1D_2(\Gamma_3)$ transition and explained by the combined effect of unresolved hyperfine structure and nonaxial crystal strains.[5]

The very first analysis of the crystal-field energies of Pr^{3+} in $CsCdBr_3$ (Ref. 1) showed that the crystal field affecting the symmetric dimer centers consists of strong cubic and weak trigonal components and that the last one is determined mainly by the quadrupolar (B_2^0) term. This conclusion was confirmed in the studies of the crystal-field energies of Tm^{3+} and Ho^{3+} symmetric pair centers where data obtained from both optical and submillimeter EPR investigations were taken into account.[6,7] The sets of crystal-field parameters obtained in Refs. 2 and 8 from the fitting of the simulated energy-level schemes to the measured 40 energy levels of Pr^{3+} are close to one another and provide small enough root-mean-square deviations (22.4–11.1 cm^{-1}) between calculated and observed energy-level data. However, some of the crystal-field parameters in $CsCdBr_3:R^{3+}$ presented in the literature,[6–9] in particular, B_6^0 and B_6^6, vary nonmonotonically with the occupation number of the $4f$-electron shell.

We have undertaken the low-temperature high-resolution infrared absorption study of $CsCdBr_3:Pr^{3+}$ with the aims (i) to determine directly positions of crystal-field levels in the

region between 2000 and 7000 cm^{-1} and (ii) to study the linewidths and line shapes and thus to obtain information on relaxation processes and hyperfine interactions. We also performed crystal-field calculations for the main center in the framework of the semiphenomenological exchange charge model (ECM),[10] based on the analysis of the local lattice structure. Parameters of the ECM were corrected by fitting the calculated hyperfine splittings of crystal field levels to the experimental data from our measurements. The electron-phonon interaction effects, in particular, the low-temperature relaxation of excited states of the $(Pr^{3+})_2$-dimer due to one- and two-phonon transitions between the crystal-field sublevels of the $^3H_5$, $^3H_6$, $^3F_2$, and $^3F_3$ multiplets, are studied in the framework of the recently derived rigid-ion model of the lattice dynamics of doped $CsCdBr_3:R$ crystals.[11]

II. EXPERIMENT

$CsCdBr_3$ crystals containing 0.2% of Pr^{3+} were grown by the method described in Ref. 12. Crystals easily cleave along the *c* axis. We have prepared a 1.3 mm thick sample (sample A) with the *c* axis parallel to the cleaved face. The sample was upheld at a controlled temperature of 5 K in a helium-vapor cryostat. Unpolarized absorption spectra were measured with a BOMEM DA3.002 Fourier transform spectrometer in the spectral range between 2000 and 7000 cm^{-1} with a resolution from 1.0 to 0.05 cm^{-1}. In Fourier transform spectroscopy, the quantity $Res=1/\mathcal{L}$, where $\mathcal{L}$ is the maximum optical path difference, is indicated as the resolution. The full width at half hight (FWHH) of the instrumental function depends on a particular apodization function used. We used no apodization and, thus, worked with the narrowest possible instrumental function (FWHH$=0.6$ Res). It is easy to show that, in this case, the shape of a spectral line is essentially unchanged provided that FWHH$\leqslant$Res.

Precision of the experimental line positions was 0.05–0.3 cm^{-1}, depending on a particular line. A precise absolute wave number scale is an intrinsic property of Fourier transform spectroscopy. Linewidths were determined from absorbance spectra calculated with a zero line taken at a half of transmitted intensity. In such a way we tried to take into consideration the fact that the incident light is unpolarized but a majority of lines is 100% polarized.

The lowest frequency region of the $^3H_4 \rightarrow {}^3F_3$ spectral transition has also been measured with the resolution of 0.005 cm^{-1} using another sample 3.1 mm thick and oriented approximately along the *c* axis (sample B). It allowed almost pure $\mathbf{k} \| c$ geometry and, consequently, $\mathbf{E},\mathbf{H} \perp c$ polarization of the incident light.

III. EXPERIMENTAL RESULTS

Figure 1 shows low-temperature transmittance spectra of $CsCdBr_3:Pr^{3+}$ (0.2%) corresponding to different infrared transitions. The first excited state of the ground multiplet $^3H_4$ lies at about 170 cm^{-1} (Refs. 1–4) and is not populated at helium temperatures. So, low-temperature absorption spectra display crystal-field levels of the excited multiplets

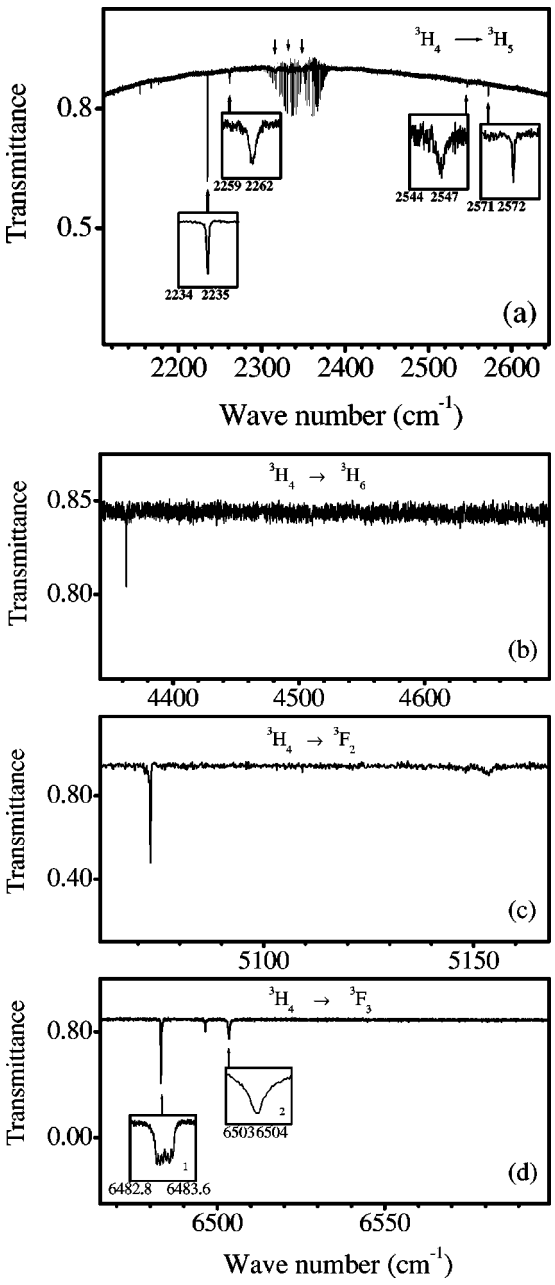

FIG. 1. Transmittance spectra of $CsCdBr_3:Pr^{3+}$ at 5 K corresponding to the optical transitions from the ground state $^3H_4(^1\Gamma_1)$ to the excited (a) $^3H_5$, (b) $^3H_6$, (c) $^3F_2$, and (d) $^3F_3$ crystal-field multiplets. The spectral resolution is 0.055, 0.3, 0.3, and 0.05 cm^{-1} for (a), (b), (c), and (d), respectively, and 0.005 cm^{-1} for inset 1 of (d). Very sharp lines in the spectral region 2300–2400 cm^{-1} are due to residual CO_2 in the spectrometer.

directly. They are listed in Table I, together with data from other publications.

As the ground state is the $^3H_4(^1\Gamma_1)$ singlet, excited Γ_1 states manifest themselves in π polarization, but Γ_3 states appear in σ polarization, while Γ_2 states are silent in the electric dipole approximation (see Table II). Magnetic dipole transitions are usually very weak, with a possible exception for the $^3H_4 \rightarrow {}^3H_5$ transition that is allowed for the free Pr^{3+} ion.

TABLE I. Positions (cm^{-1}) and symmetries of energy levels for the symmetric dimer centers and widths (in parentheses, cm^{-1}) of absorption lines from the ground state in $CsCdBr_3:Pr^{3+}$.

	Measured					
Multiplet	This work		Literature data (Refs. 1–4)		Calculated	
$^3H_4$	0		0	Γ_1	0	$^1\Gamma_1$
			166–170	Γ_2, Γ_3 ?	168	$^1\Gamma_3$
			194–196	Γ_3, Γ_2 ?	188	Γ_2
			323–328	Γ_3	293	$^2\Gamma_3$
			551–555	Γ_1	545	$^2\Gamma_1$
			574–580	Γ_3	564	$^3\Gamma_3$
$^3H_5$	2234.8 (0.05)	Γ_1, Γ_2?	2230–2236	Γ_2	2235	$^1\Gamma_2$
	2261.4 (0.64)	Γ_3	2256–2264	Γ_3	2251	$^1\Gamma_3$
	2316.5 (3.0)	Γ_1, Γ_3?	2309–2318	Γ_1, Γ_3?	2330	$^2\Gamma_3$
	2331.9 (3.3)	Γ_3, Γ_1?	2327–2334	Γ_3, Γ_1?	2334	Γ_1
	2348.4 (3.7)		2347			
	2546.7 (0.7)	Γ_3	2533–2547	Γ_3	2540	$^3\Gamma_3$
			2544–2595	Γ_2	2593	$^2\Gamma_2$
					2620	$^4\Gamma_3$
$^3H_6$	4362.8 (0.19)	Γ_3	4362–4364	Γ_3	4363	$^1\Gamma_3$
			4374–4378	Γ_1	4390	$^1\Gamma_1$
			4413–4415	Γ_3	4414	$^2\Gamma_3$
			4494	Γ_2	4539	$^1\Gamma_2$
			4700–4704	Γ_3	4710	$^3\Gamma_3$
			4725–4730	Γ_1	4733	$^2\Gamma_1$
			4761	Γ_3	4765	$^4\Gamma_3$
			4781–4808	Γ_2	4804	$^2\Gamma_2$
			4808–4843	Γ_1	4815	$^3\Gamma_1$
$^3F_2$	5073.0 (0.11)	Γ_3	5070–5076	Γ_3	5073	$^1\Gamma_3$
			5145–5153	Γ_1, Γ_3 ?	5128	$^2\Gamma_3$
	5153.5 (2.8)		5152–5158	Γ_1	5136	Γ_1
$^3F_3$			6473–6479	Γ_2	6473	$^1\Gamma_2$
	6483.3 (0.26)	Γ_3	6480–6488	Γ_3	6483	$^1\Gamma_3$
	6496.5 (0.17)	Γ_1	6499–6500	Γ_1	6485	Γ_1
	6503.5 (0.4)	Γ_3	6500–6510	Γ_3	6495	$^2\Gamma_3$
			6526–6535	Γ_2	6533	$^2\Gamma_2$
$^3F_4$	6858.0 (<1)		6858–6860	Γ_1	6858	$^1\Gamma_1$
			6894	Γ_2	6907	Γ_2
			6903–6908	Γ_3	6902	$^1\Gamma_3$
			6914	Γ_3	6930	$^2\Gamma_3$
			7103–7104	Γ_1	7115	$^2\Gamma_1$
			7111–7117	Γ_3	7108	$^3\Gamma_3$
$^1G_4$			9777		9777	$^1\Gamma_1$
					9869	$^1\Gamma_3$
					9899	Γ_2
					9955	$^2\Gamma_3$
					10427	$^2\Gamma_1$
					10453	$^3\Gamma_3$
$^1D_2$			16536–16540	Γ_3	16536	$^1\Gamma_3$
			16567–16570	Γ_1	16588	Γ_1
			17004–17011	Γ_3	17001	$^2\Gamma_3$
$^3P_0$			20386–20393	Γ_1		
$^3P_1$			20956–20964	Γ_2	20964	Γ_2
			21011–21047	Γ_3	21010	Γ_3
$^3P_2$			22106–22118	Γ_3	22117	$^1\Gamma_3$
			22163–22177	Γ_1	22165	Γ_1
			22216–22229	Γ_3	22223	$^2\Gamma_3$

TABLE II. Selection rules for electric dipole (d) and magnetic dipole (μ) transitions in the C_{3v} point group.

C_{3v}	Γ_1	Γ_2	Γ_3
Γ_1	d_z	μ_z	$d_x, d_y; \mu_x, \mu_y$
Γ_2	μ_z	d_z	$d_x, d_y; \mu_x, \mu_y$
Γ_3	$d_x, d_y; \mu_x, \mu_y$	$d_x, d_y; \mu_x, \mu_y$	$d_z; d_x, d_y; \mu_x, \mu_y$

The symmetries of the $^3F_3$ crystal-field levels have been determined from a comparison between the spectra of the two differently oriented samples (samples A and B). The assignment of the 6483.3 cm^{-1} level as a Γ_3 level is strongly supported by the well-resolved hyperfine structure (hfs) observed in high-resolution spectra [see inset 1 of Fig. 1(d) and Fig. 2(a)]. The point is that while Γ_3 levels exhibit the magnetic hfs, Γ_1 and Γ_2 do not. The next Γ_3 level also shows the traces of unresolved hfs, namely, the 6503.5 cm^{-1} line has a flat bottom [see inset 2 of Fig. 1(d)].

Expansion of the 6483.3 cm^{-1} line into six components yields 0.040 cm^{-1} wide Gaussians. The Gaussian shape of hfs components gives evidence that an inhomogeneous broadening due to random crystal fields exceeds a homogeneous broadening due to nonradiative transitions to the nearest $^1\Gamma_2$ level lying at about 10 cm^{-1} lower[1,2] (we did not observe $^3H_4(^1\Gamma_1) \rightarrow {}^3F_3(\Gamma_2)$ transitions forbidden as electric dipole ones). The line shapes of the 6496.5 cm^{-1} ($\Gamma_1 \rightarrow \Gamma_1$) and 6503.5 cm^{-1} ($\Gamma_1 \rightarrow \Gamma_3$) lines reveal homogeneous broadening of 0.17 and 0.31 cm^{-1}, respectively. Such a broadening comes, evidently, from the electron-phonon interaction and implies a noticeable density of phonon states in the region between 20 and 30 cm^{-1}, corresponding to the distances from the considered levels to lower crystal-field levels.

Other examples of level broadening due to the electron-phonon interaction can be found in the $^3H_5$ multiplet which is situated in the region of about 2400 cm^{-1} [see Fig. 1(a)]. The lowest level of this multiplet lying at about 2234 cm^{-1} was reported to be the $^1\Gamma_2$ level, from polarized fluorescence measurements.[1] In that case, a strong very narrow (with the width of 0.05 cm^{-1}) line observed at 2234.8 cm^{-1} corresponds to the magnetic dipole transition $^3H_4(^1\Gamma_1) \rightarrow {}^3H_5(^1\Gamma_2)$. As we have already mentioned, such a situation is possible just for the $^3H_4 \rightarrow {}^3H_5$ spectral multiplet. The next level lies at 26 cm^{-1} from the bottom of the multiplet and, although it suffers from a phonon relaxation, exhibits hfs as it follows from the shape of 2261.4 cm^{-1} line. This is in accordance with the previously made assignments of this level symmetry as Γ_3. Three closely spaced levels at 2316.6, 2331.9, and 2347.8 cm^{-1} are broad. Their widths are 3.0, 3.3, and 3.7 cm^{-1}, respectively, and it is not possible to determine their symmetries. Calculations described below show that an overall hyperfine splittings of Γ_3 levels do not exceed 0.5 cm^{-1}. Consequently, the level widths of 3–4 cm^{-1} are mainly due to rapid phonon-assisted decay to lower levels. In accordance with the crystal-field calculations (see below), at least one of these three broad absorption lines is to be assigned to another center. The next level is more narrow again. According to the shape of the line at 2546.7 cm^{-1} it contains unresolved hfs and thus corresponds to the Γ_3 level. The distances from this level to lower levels exceed the length of the phonon spectrum [$\sim$180 cm^{-1} (Ref. 11)]. Consequently one-phonon relaxation is not possible.

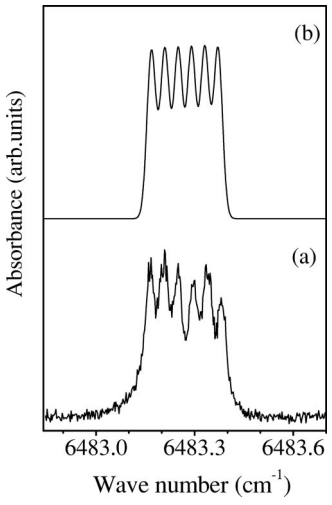

FIG. 2. (a) Measured hyperfine structure with resolution 0.005 cm^{-1} and (b) calculated hyperfine structure of the $^3H_4(^1\Gamma_1) \rightarrow {}^3F_3(^1\Gamma_3)$ transition of $CsCdBr_3:Pr^{3+}$.

The highest frequency line observed at 2572.1 cm^{-1} could be attributed to the $^3H_4(^1\Gamma_1) \rightarrow {}^3H_5(^2\Gamma_2)$ magnetic dipole transition. But the $^3H_5(^2\Gamma_2)$ level lying at 26 cm^{-1} above the $^3H_5(^3\Gamma_3)$ level (2546 cm^{-1}) should be broadened due to one- and two-phonon transitions to the lower crystal-field sublevels, and the width of the respective spectral line should be about 0.3–0.5 cm^{-1} (see Table III), not 0.05 cm^{-1} as observed. Probably, this line belongs to some other Pr^{3+} center. Weak narrow lines observed at 2153.6 and 2167.3 cm^{-1} [see Fig. 1(a)] also have to be assigned to some other centers. If these levels belonged to the main center, the level at 2234.8 cm^{-1} would be broadened by the nonradiative transitions to these levels. It is not the case experimentally.

We were able to find only two levels in the $^3F_2$ multiplet and the lowest sublevel in each of $^3F_4$ and $^3H_6$. The level at 5073 cm^{-1}, which lies far (250 cm^{-1}) from a lower level, is evidently broadened by unresolved hfs and is thus a Γ_3 level. The measured hyperfine splittings and widths of hyperfine sublevels found from the experimental line shapes are presented in Table III, to compare with the calculated hyperfine splittings and the estimated one-phonon decay rates (see the next section).

Many of the observed levels coincide with those of Refs. 1–4 found from selectively excited fluorescence measurements. We did not observe any additional structure due to nonequivalence of Pr^{3+} positions in asymmetric pair centers. Thus, our results support the conclusion of Refs. 1–3 that the main center in $CsCdBr_3:Pr^{3+}$ is a symmetric pair [Pr^{3+}–Cd^{2+} vacancy–Pr^{3+}].

IV. CRYSTAL-FIELD CALCULATIONS

The energy-level pattern of the $^{141}Pr^{3+}$ ion (the nuclear spin $I=5/2$, 100% abundant, the $4f^2$ electron shell) in the

TABLE III. The calculated and measured total hyperfine structure widths $\Delta E/\hbar$, the one-phonon relaxation rates W, and the widths $\Delta\omega$ (10^{10} s^{-1}) of the crystal-field sublevels at the temperature of 5 K.

$^{2S+1}L_J$	Crystal-field energy (cm^{-1})	$\Delta E/\hbar$		W [a]	$\Delta\omega$
		Calculated	Measured	Calculated	Measured
$^3H_5$	$^1\Gamma_2$ 0 (2235)	0.05	<0.94	0	0.94[b]
	$^1\Gamma_3$ 26	6.68	6.41	15.5 [113]	5.65
	$^2\Gamma_3$ 82	5.43		255 [573]	56.6
	$^1\Gamma_1$ 97	0.16		157 [745]	62.2
	$^3\Gamma_3$ 312	2.65		7.2[c]	13.2
	$^2\Gamma_2$ 358	0		52 [59]	
	$^4\Gamma_3$ 385	9.03		59 [311]	
$^3H_6$	$^1\Gamma_3$ 0 (4363)	2.00	2.26	0	1.30[b]
$^3F_2$	$^1\Gamma_3$ 0 (5073)	1.15	1.32	0	0.94[b]
	$^2\Gamma_3$ 75	2.09		14 [31]	
	$^1\Gamma_1$ 80	0.03		32 [57]	52.8
$^3F_3$	$^1\Gamma_2$ 0 (6473)	0.03		0	
	$^1\Gamma_3$ 10	3.71	3.96	0.52 [9.0]	0.75[b]
	$^1\Gamma_1$ 23	0		4.5 [26]	3.20
	$^2\Gamma_3$ 30	1.53	1.69	15.8 [95]	5.85
	$^2\Gamma_2$ 53	0		63 [98]	

[a]Numbers in square brackets were obtained with the phonon spectrum of the unperturbed crystal lattice.
[b]The inhomogeneous width.
[c]Two-phonon relaxation rate.

trigonal crystal field can be represented by eigenvalues of the effective parametrized Hamiltonian

$$H = V_{ee} + H_{so} + \Delta E(L,S,J) + H_{cf} + H_{hf}, \tag{1}$$

where V_{ee} is the two-body Coulomb energy; H_{so} corresponds to the spin-orbit interaction [we use in the present work $\zeta = 746.2$ cm^{-1} and Slater integrals $F_2 = 304.4$; $F_4 = 45.47$; $F_6 = 4.41$ cm^{-1} (Ref. 13)]; H_{cf} is the crystal-field Hamiltonian

$$H_{cf} = B_2^0 O_2^0 + B_4^0 O_4^0 + B_4^3 O_4^3 + B_6^0 O_6^0 + B_6^3 O_6^3 + B_6^6 O_6^6 \tag{2}$$

(O_p^k are the Stevens operators,[10] and the quantization axis z coincides with the symmetry axis C_3 of the crystal lattice), and H_{hf} is the energy of the electron-nuclear interaction responsible for the hyperfine structure of the optical spectra. Because we neglect many minor interactions (three-body terms, spin–other-orbit interaction, two-body correlations in the crystal-field terms, etc.), shifts of the multiplet centers of gravity $\Delta E(L,S,J)$ are introduced to fit the calculated spectrum to the experimental data. Only projections of the electron-nuclear magnetic dipole and electric quadrupolar interactions on multiplet manifolds with fixed orbital (L), spin (S), and total (J) angular moments were considered:

$$\begin{aligned} H_{hf} = {} & A(L,S,J)\mathbf{J}\cdot\mathbf{I} + \frac{e^2Q(1-\gamma)}{4I(2I-1)}V_{zz}[3I_z^2 - I(I+1)] \\ & - \frac{3e^2Q\langle r^{-3}\rangle\alpha_J}{4I(2I-1)}\left[\frac{1}{3}[3J_z^2 - J(J+1)][3I_z^2 - I(I+1)]\right. \\ & + \frac{1}{2}[J_+^2 I_-^2 + J_-^2 I_+^2] + \frac{1}{2}(J_z J_+ + J_+ J_z)(I_z I_- + I_- I_z) \\ & \left. + \frac{1}{2}(J_z J_- + J_- J_z)(I_z I_+ + I_+ I_z)\right]. \end{aligned} \tag{3}$$

Here $A(L,S,J)$ is the magnetic dipole hyperfine constant [in the free ion $A(^3H_4) = 1.093$ GHz,[14] the corresponding hyperfine constants for other multiplets are obtained using this value and neglecting the core electron polarization contributions that do not exceed 1.5% of the $4f$ electron contributions[15]], $Q = -5.9\times10^{-30}$ m^2 (Ref. 14) is the nuclear quadrupole moment, $\gamma = -70\pm10$ is the Sternheimer antishielding factor,[16] α_J are reduced matrix elements of the second-rank spherical operators, $\langle r^p\rangle$ are moments of the radial wave function of the $4f$ electrons calculated in Ref. 17, and the electric field gradient at the Pr^{3+} nucleus is

$$eV_{zz} = \sum_i eq(i)\frac{3\cos^2\theta(i) - 1}{R(i)^3}, \tag{4}$$

where $q(i)$ is the charge (in units of the proton charge e) of a lattice ion with spherical coordinates $R(i)$, $\theta(i)$, and $\varphi(i)$ in the system of coordinates having its origin at the Pr^{3+} nucleus.

TABLE IV. Crystal-field parameters B_p^k (cm^{-1}) of symmetric dimer centers in $CsCdBr_3:R^{3+}$ crystals.

p	k	Tm ($4f^{12}$) (Ref. 6)	Ho ($4f^{10}$) (Ref. 7)	Nd ($4f^3$) (Ref. 9)	Pr ($4f^2$) (Ref. 8)	This work (a)	This work (b)
2	0	−81.4	−75.6	−102	−79	−72.3	−70
4	0	−82.0	−94.3	−121	−149	−128.8	−140.6
4	3	2362	2841	3698	4044	4115	4191
6	0	11.26	12.75	14.06	22.62	14.95	15.1
6	3	153	216	342	347	164	279
6	6	106	150	187	37	229	101

As we have already mentioned in the Introduction, the crystal-field parameters, obtained earlier from the fitting to the measured energy levels of Pr^{3+} (Refs. 2 and 8) and Nd^{3+} (Ref. 9) in $CsCdBr_3$, though providing small enough deviations between the calculated and observed energy levels, exhibit nonmonotonic variation within the R^{3+} family (see Table IV). Moreover, there are large discrepancies between the measured in this work hfs of the absorption lines and the hfs calculated with the crystal-field parameters from Ref. 8. In particular, the 6483 cm^{-1} line exhibits a well-resolved hfs of total width 0.21 cm^{-1}, while the calculated width is 0.11 cm^{-1}. The formal fitting procedure employed in Refs. 2, 8, and 9 evidently brings about overestimated six-rank parameters of the trigonal crystal-field component.

To clear up relations between the crystal-field parameters and their origin, we estimated them in the framework of the exchange charge model.[10] The crystal field is represented as a sum ($B_p^k = B_{pq}^k + B_{pS}^k$) of the electrostatic field of the lattice ions and the exchange charge field defined by the parameters

$$B_{pq}^k = -e^2 K_p^k (1-\sigma_p)\langle r^p\rangle \sum_i q(i)\frac{O_p^k(\theta(i),\varphi(i))}{R(i)^{p+1}} \quad (5)$$

and

$$B_{pS}^k = \frac{2(2p+1)}{7} e^2 K_p^k \sum_i [G_s S_s(i)^2 + G_\sigma S_\sigma(i)^2 + \gamma_p G_\pi S_\pi(i)^2]\frac{O_p^k(\theta(i),\varphi(i))}{R(i)}, \quad (6)$$

respectively. Here K_p^k are numerical factors,[10] σ_p are the shielding factors, $\gamma_2 = 3/2$, $\gamma_4 = 1/3$, $\gamma_6 = -3/2$, and G_s and $G_\sigma = G_\pi = G_p$ are dimensionless parameters of the model. Expression (6) involves the sum over only the nearest neighbors (six bromine ions) of the R^{3+} ion. The overlap integrals $S_s = \langle 4f, m=0 | 4s\rangle$, $S_\sigma = \langle 4f, m=0 | 4p, m=0\rangle$, and $S_\pi = \langle 4f, m=1 | 4p, m=1\rangle$ have been computed using the radial $4f$ wave function of the Pr^{3+} ion from Ref. 17 and the $4s$, $4p$ wave functions of the Br^- ion given in Ref. 18. Dependences of the overlap integrals on the interionic distance R (in ångstroms) are approximated by the following expressions:

$$S_s = 0.09988 \exp(-0.20882 R^{2.17238});$$

$$S_\sigma = 0.04610 \exp(-0.03733 R^{3.0662}); \quad (7)$$

$$S_\pi = 0.39635 \exp(-0.87514 R^{1.30253}).$$

Equations (5)–(7) present the crystal-field parameters as explicit functions of relative positions of the impurity Pr^{3+} ion and the lattice ions. We analyzed distortions in the relaxed $CsCdBr_3$ lattice containing the substitutional dimer [Pr^{3+}–Cd^{2+} vacancy–Pr^{3+}] in the framework of the same quasimolecular model as the one already used in Ref. 6 to calculate the structure of symmetric Tm^{3+} dimers. Values of ion displacements from their equilibrium positions in the perfect lattice were obtained by minimizing the potential energy of the cluster, which involved the nearest 50 ions around the symmetric dimer center. These ions belong to the first (12 Br^-), second (2 Cd^{2+}), third (12 Cs^+), and fourth (24 Br^-) coordination shells of the impurity Pr^{3+} ions (see Table V).

The energy of the interionic interaction is assumed to be a sum of Coulomb and non-Coulomb terms. The effective ion charges [$q(Cd^{2+}) = 1.56$, $q(Cs^+) = 0.84$, $q(Br^-) = -0.8$, $q(Pr^{3+}) = 2.34$] and the non-Coulomb force constants, corresponding to interactions between the nearest neighbors, Pr^{3+}-Br^-, Cd^{2+}-Br^-, Cs^+-Br^-, and Br^--Br^-, have been obtained from the study of the $CsCdBr_3$ lattice dynamics.[11] According to results of simulating the relaxation energy minimum with respect to the ion displacements (see Table V), the distance between the Pr^{3+} ions attracted by the Cd^{2+} vacancy diminishes from the value of the lattice constant $c = 0.6722$ nm (Ref. 19) down to 0.5915 nm. This value is very close to the distance of 0.593 nm between the Gd^{3+} ions[20] and 0.5943 nm between the Tm^{3+} ions[6,21] in the symmetric pair centers in $CsCdBr_3$, as determined from the EPR spectra. In the perfect lattice, the first coordination shell of a Cd^{2+} ion has a radius of 0.277 nm; in the symmetric dimer center six Br^- ions nearest to the Cd^{2+} vacancy are forced outwards, but the displacements of the Pr^{3+} ions along the dimer axis are so large that the corresponding Pr^{3+}-Br^- distance decreases down to 0.275 nm. In contrast, the terminal triangles of the Br^- ions lag behind the impurity ions and the corresponding interionic distance increases up to 0.290 nm. These values agree with the distances (0.264

TABLE V. Structure of the symmetric dimer Pr^{3+}–Cd^{2+} vacancy–Pr^{3+} [lattice constants $a=0.7675$ nm; $c=0.6722$ nm; $\nu=0.1656$ (Ref. 19)].

Ion	Coordinates x/a	y/a	z/c
$(Pr^{3+})_{1,2}$	0	0	$\pm[0.5-0.06003]$
$(Br^{-})_{1,4}$	$\pm[\sqrt{3}\nu-0.01032]$	0	$\pm[0.75-0.01400]$
$(Br^{-})_{2,5}$	$\pm[-\sqrt{3}\nu+0.01032]/2$	$\pm\sqrt{3}[\sqrt{3}\nu-0.01032]/2$	$\pm[0.75-0.01400]$
$(Br^{-})_{3,6}$	$\pm[-\sqrt{3}\nu+0.01032]/2$	$\pm\sqrt{3}[-\sqrt{3}\nu+0.01032]/2$	$\pm[0.75-0.01400]$
$(Br^{-})_{7,10}$	$\pm[-\sqrt{3}\nu-0.03022]$	0	$\pm[0.25-0.00152]$
$(Br^{-})_{8,11}$	$\pm[\sqrt{3}\nu+0.03022]/2$	$\pm\sqrt{3}[-\sqrt{3}\nu-0.03022]/2$	$\pm[0.25-0.00152]$
$(Br^{-})_{9,12}$	$\pm[\sqrt{3}\nu+0.03022]/2$	$\pm\sqrt{3}[\sqrt{3}\nu+0.03022]/2$	$\pm[0.25-0.00152]$
$(Cs^{+})_{1,4}$	$\pm[-1/\sqrt{3}-0.02051]$	0	$\pm[0.75+0.00469]$
$(Cs^{+})_{2,5}$	$\pm[1/\sqrt{3}+0.02051]/2$	$\pm\sqrt{3}[-1/\sqrt{3}-0.02051]/2$	$\pm[0.75+0.00469]$
$(Cs^{+})_{3,6}$	$\pm[1/\sqrt{3}+0.02051]/2$	$\pm\sqrt{3}[1/\sqrt{3}+0.02051]/2$	$\pm[0.75+0.00469]$
$(Cs^{+})_{7,10}$	$\pm[1/\sqrt{3}-0.00602]$	0	$\pm[0.25-0.01938]$
$(Cs^{+})_{8,11}$	$\pm[-1/\sqrt{3}+0.00602]/2$	$\pm\sqrt{3}[1/\sqrt{3}-0.00602]/2$	$\pm[0.25-0.01938]$
$(Cs^{+})_{9,12}$	$\pm[-1/\sqrt{3}+0.00602]/2$	$\pm\sqrt{3}[-1/\sqrt{3}+0.00602]/2$	$\pm[0.25-0.01938]$
$(Cd^{2+})_{1,2}$	0	0	$\pm[1-0.00290]$
$(Br^{-})_{13-16}$	$\pm[-\sqrt{3}(\nu-0.5)+0.00404]$	$\pm[\pm(0.5+0.00532)]$	$\pm[0.25+0.00231]$
$(Br^{-})_{17-20}$	$\pm[0.5\sqrt{3}\nu+0.00258]$	$\pm[\pm(1.5\nu-1-0.00616)]$	$\pm[0.25+0.00231]$
$(Br^{-})_{21-24}$	$\pm[0.5\sqrt{3}(\nu-1)-0.00662]$	$\pm[\pm(1.5\nu-0.5-0.00084)]$	$\pm[0.25+0.00231]$
$(Br^{-})_{25-28}$	$\pm[\sqrt{3}(\nu-0.5)+0.00151]$	$\pm[\pm(0.5-0.00288)]$	$\pm[0.75+0.00058]$
$(Br^{-})_{29,32}$	$\pm[-0.5\sqrt{3}\nu+0.00174]$	$\pm[\pm(1.5\nu-1+0.00275)]$	$\pm[0.75+0.00058]$
$(Br^{-})_{33-36}$	$\pm[0.5\sqrt{3}(1-\nu)-0.00325]$	$\pm[\pm(1.5\nu-0.5-0.00013)]$	$\pm[0.75+0.00058]$

and 0.286 nm) between the Yb^{3+} and the nearest Br^{-} ions in the intrinsic dimer units in $Cs_3Yb_2Br_9$.[22]

Taking into account the local lattice deformation, we obtained from Eqs. (5)–(7) the following crystal-field parameters (values are in cm^{-1}) for Pr^{3+} ion in the symmetric dimer center [the electrostatic contribution to the quadrupolar crystal-field component $B^0_{2q}=-e^2(1-\sigma_2)\langle r^2\rangle V_{zz}/4$ was computed exactly with the Ewald method]:

$$B^0_2=-445.5(1-\sigma_2)-1.123G_s-2.828G_p;$$

$$B^0_4=-42.7(1-\sigma_4)-4.52G_s-10.12G_p;$$

$$B^3_4=1184(1-\sigma_4)+156.84G_s+341.60G_p;$$

$$B^0_6=1.68(1-\sigma_6)+1.96G_s+0.4395G_p;$$

$$B^3_6=13.4(1-\sigma_6)+12.56G_s+13.56G_p;$$

$$B^6_6=24.9(1-\sigma_6)+27.61G_s+9.06G_p.$$

Values of the model parameters $G_s=5.4$; $G_p=6.1$ have been determined by comparing the calculated and measured total splittings of the ground state $^3H_4$ and of the excited multiplet $^3H_6$, the shielding factors have been fixed at $\sigma_4=\sigma_6=0$, $\sigma_2=0.89$ in accordance with the theoretical estimations.[16] The crystal-field parameters so obtained [column (a) of Table IV] were used as starting values for the fitting procedure constrained by the additional conditions that the calculated hfs had to agree with the experimental data.

The final values of the crystal-field parameters for the Pr^{3+} centers as compared with the corresponding parameters of Tm^{3+}, Ho^{3+}, and Nd^{3+} centers are given in column (b) of Table IV. Despite the large trigonal distortion of the nearest bromine octahedron, the main features of the crystal-field splittings are determined by the cubic component of the crystal field. The B^3_6 and B^6_6 parameters involve the largest changes from the initial (calculated) to the final (fitted) values. These differences are most probably caused by the overestimated displacements of the six Br_7-Br_{12} ions in the basis plane (see Table V). The calculated energy levels of the Pr^{3+} ions presented in Table I were obtained by diagonalizing the Hamiltonian (1) in the space of 516 states (terms ^3H, ^3F, ^3P, ^1I, ^1G, ^1D were taken into account) with fitted barycenters of the free-ion multiplets. The measured splittings of the $^3H_4$, $^3H_5$, $^3H_6$, $^3F_2$, $^3F_3$, $^3F_4$, $^3P_1$, $^3P_2$, $^1D_2$ multiplets of Pr^{3+} are satisfactorily described by our final set of crystal-field parameters [column (b) in Table IV].

The computed hfs of Γ_1 and Γ_2 crystal-field singlets consists of three doublets with the total width ΔE of no more than 0.02 cm^{-1}, which cannot be resolved in the optical spectra. The quadrupolar contributions to the hfs are very small ($\sim 10^{-4}$ cm^{-1}); the calculated hfs of Γ_3 doublets is actually equidistant with intervals of no more than 0.1 cm^{-1}. An example of the simulated envelope of the absorption line $^3H_4(^1\Gamma_1)\rightarrow{}^3F_3(^1\Gamma_3)$, where individual

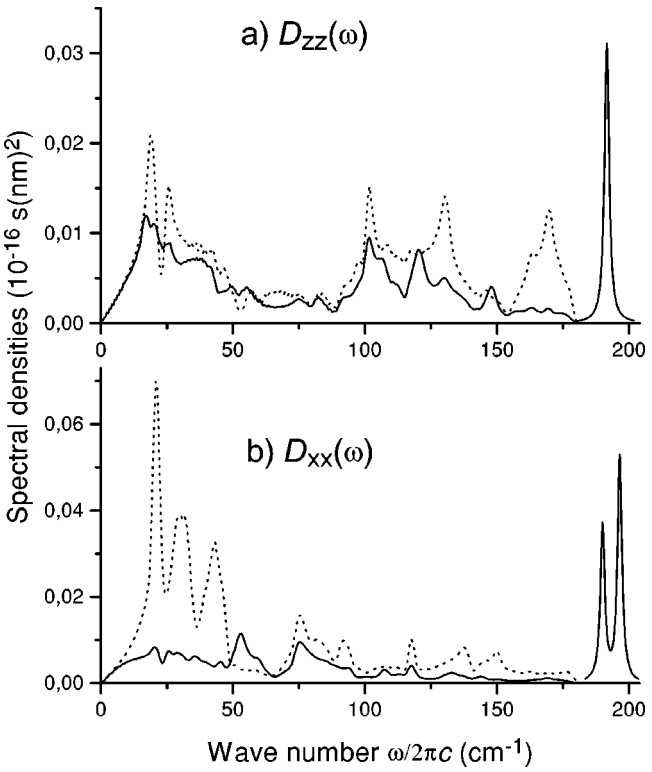

FIG. 3. Simulated spectral densities of displacement-displacement autocorrelation functions for Cd^{2+} in $CsCdBr_3$ (dotted curves) and for Pr^{3+} in the impurity dimer centers (solid curves).

transitions between different electron-nuclear states are presented by Gaussians of 0.04 cm^{-1} width, is given in Fig. 2(b). The observed irregular shape of the hfs of some absorption lines [see Fig. 2(a) and Ref. 5] is most probably caused by crystal fields of low symmetry. We discussed this point in more detail in another publication.[23]

The most essential difference between results of our calculations and fitting procedures performed in Refs. 2 and 8 is connected with assignments of symmetry types of some crystal-field energy levels. In particular, symmetries of the third ($^2\Gamma_3$) and fourth (Γ_1) sublevels of the $^3H_5$ multiplet and of the second ($^1\Gamma_3$) and third (Γ_2) sublevels of the ground $^3H_4$ multiplet are inverted in Refs. 2 and 8 (it should be noted that our scheme of crystal-field energies of the ground state agrees with the assignment of Ref. 4). Additional measurements of polarized spectra are to be carried out to check our predictions.

V. RELAXATION BROADENING OF THE CRYSTAL-FIELD LEVELS

Even at the liquid-helium temperature the hfs of the most of excited crystal-field sublevels is masked by the spontaneous relaxation broadening. Strong electron-phonon interaction effects in $CsCdBr_3:R^{3+}$ crystals originate from the specific density of phonon states that has large maxima in the low-frequency region (20–40 cm^{-1}) in the perfect crystal lattice (see Fig. 3 and Ref. 11). The Hamiltonian of the electron-phonon interaction, expanded in a power series in ion displacements from their equilibrium positions, can be written as follows:

$$H_{\text{el-ph}}=\sum_{s\alpha} V_\alpha(s)[u_\alpha(s)-u_\alpha(R)] + \frac{1}{2}\sum_{s\alpha\beta} V_{\alpha\beta}(s)[u_\alpha(s)-u_\alpha(R)] \times[u_\beta(s)-u_\beta(R)]\cdots, \tag{8}$$

$$V_\alpha(s)=\sum_{pk} B^k_{p,\alpha}(s)O^k_p, \quad V_{\alpha\beta}(s)=\sum_{pk} B^k_{p,\alpha\beta}(s)O^k_p,$$

where $[\mathbf{u}(s)-\mathbf{u}(R)]$ is the difference between dynamic displacements of the ligand ion s and the R ion, and $B^k_{p,\alpha}(s)$ and $B^k_{p,\alpha\beta}(s)$ are the coupling constants. The probability of the one-phonon transition between the initial (i) and final (f) states of the R ion with the energy gap $\hbar\omega_{if}>0$ can be represented as

$$W_{if}=\frac{2}{\hbar}\sum_{s\alpha s'\beta}\langle f|V_\alpha(s)|i\rangle \mathrm{Im}\, g_{\alpha\beta}(ss'|\omega_{if}) \times\langle i|V_\beta(s')|f\rangle[1+n(\omega_{if})], \tag{9}$$

where $n(\omega)$ is the phonon occupation number, and $g_{\alpha\beta}(ss'|\omega)$ are spectral representations of the Green's functions for differences between the ion displacements.[24] We performed a calculation of the relaxation rates for all the crystal-field sublevels within the manifolds of $^3H_5$, $^3F_2$, and $^3F_3$ multiplets using the phonon Green's functions of the perfect ($CsCdBr_3$) and locally perturbed (impurity dimer centers in $CsCdBr_3:Pr^{3+}$) crystal lattices obtained in Ref. 11. The formation of a dimer leads to a strong perturbation of the crystal lattice (mass defects in the three adjacent Cd^{2+} sites and large changes of force constants). As it has been shown in Ref. 11, the local spectral density of phonon states essentially redistributes and several localized modes corresponding to different representations of the dimer point symmetry group D_{3d} appear near the boundary of the continuous phonon spectrum of the unperturbed lattice. As an example of changes in the phonon spectrum, we present in Fig. 3 spectral densities $D_{\alpha\alpha}(\omega)$ of displacement-displacement autocorrelation functions

$$\langle u^2_\alpha(R)\rangle=\int D_{\alpha\alpha}(\omega)d\omega, \tag{10}$$

in the perfect ($R=Cd^{2+}$) and perturbed ($R=Pr^{3+}$) lattices at zero temperature. The contributions to $D_{xx}(\omega)$ from the localized modes of Γ_{3g} (196.5 cm^{-1}) and Γ_{3u} (190 cm^{-1}) symmetry, and to $D_{zz}(\omega)$ from the localized modes of Γ_{1g} (191.7 cm^{-1}) and Γ_{2u}(191.2 cm^{-1}) symmetry, are presented by Lorentzians with the proper weights and the full width of 2 cm^{-1}.

We took into account interactions of Pr^{3+} ion with its nearest neighbors (six Br^- ions) only. Values of coupling constants were computed in the framework of the ECM with

the same parameters as those used in the crystal-field calculations (explicit expressions of the $B^k_{p,\alpha}(s)$, $B^k_{p,\alpha\beta}(s)$ are given in Refs. 10 and 24). Matrix elements of electron operators $V_\alpha(s)$ were calculated with the eigenfunctions of the Hamiltonian (1). Calculated inverse lifetimes $1/\tau_i = W_i = \Sigma_f W_{if}$ (the sum is over states *f*, which belong to the same multiplet as the crystal field level *i*, with lower energies) are given in Table III. It is seen that despite many simplifying approximations there is a good correlation between the measured linewidths and the relaxation rates obtained with the perturbed Green's functions. Calculations with Green's functions of the perfect lattice gave overestimated (up to an order of magnitude higher) values of relaxation rates. Thus, we conclude that the increased Pr^{3+}-ligand elastic interaction, as compared to the Cd^{2+}-Br^- interaction, and corresponding enhancement of correlations between displacements of the impurity R^{3+} ion and its neighbors strongly suppress the electron-phonon coupling.

It should be noted that the measured width of the doublet $^3\Gamma_3(^3H_5)$ is 5 times larger than the estimated total hfs width, though the one-phonon relaxation broadening of this level is not possible at low temperatures. We suppose that this level, and two upper levels $^2\Gamma_2(^3H_5)$ and $^4\Gamma_3(^3H_5)$ are essentially broadened due to the two-phonon relaxation. The probability of the spontaneous emission of two phonons contains three terms that correspond to the first-order contribution from the nonlinear electron-phonon interaction,

$$W^{(2a)}_{if} = \frac{1}{\pi} \sum_{s\alpha\beta s'\gamma\delta} \langle f|V_{\alpha\beta}(s)|i\rangle\langle i|V_{\gamma\delta}(s')|f\rangle \times \int\int \mathrm{Im}\, g_{\alpha\gamma}(ss'|\omega_1)\mathrm{Im}\, g_{\beta\delta}(ss'|\omega_2) \times \delta(\omega_{if}-\omega_1-\omega_2)d\omega_1 d\omega_2, \quad (11)$$

to the second-order contribution from the linear electron-phonon interaction

$$W^{(2b)}_{if} = \frac{2}{\pi\hbar^2} \sum_{jl} \int\int \left(\frac{M^{fj}_{lf}(\omega_1)M^{ji}_{il}(\omega_2)}{(\omega_{ij}-\omega_1)(\omega_{il}-\omega_1)} + \frac{M^{fj}_{il}(\omega_1)M^{ji}_{lf}(\omega_2)}{(\omega_{ij}-\omega_1)(\omega_{il}-\omega_2)} \right) \times \delta(\omega_{if}-\omega_1-\omega_2)d\omega_1 d\omega_2, \quad (12)$$

where

$$M^{fj}_{lm}(\omega_n) = \sum_{ss'\alpha\beta} \langle f|V_\alpha(s)|j\rangle \mathrm{Im}\, g_{\alpha\beta}(ss'|\omega_n)\langle l|V_\beta(s')|m\rangle, \quad (13)$$

and to the combined action of the first- and second-order transition amplitudes:

$$W^{(2c)}_{if} = \frac{2}{\pi\hbar} \sum_{s's''\gamma\delta} \sum_{\alpha\beta s,j} [\langle f|V_{\alpha\beta}(s)|i\rangle\langle i|V_\delta(s'')|j\rangle \times \langle j|V_\gamma(s')|f\rangle + \text{c.c.}] \times \int\int \mathrm{Im}\, g_{\alpha\gamma}(ss'|\omega_1)\mathrm{Im}\, g_{\beta\delta}(ss''|\omega_2) \times \frac{1}{(\omega_{ij}-\omega_1)} \delta(\omega_{if}-\omega_1-\omega_2)d\omega_1 d\omega_2. \quad (14)$$

The calculated sum of two-phonon relaxation rates $\Sigma_f W^{(2a)}_{if}$ corresponding to spontaneous transitions from the doublet $^3\Gamma_3(^3H_5)$ to all lower sublevels of the $^3H_5$ multiplet, induced by the nonlinear terms in Eq. (8), equals 1.8×10^{10} s^{-1} and is almost exactly canceled by the contribution -1.7×10^{10} s^{-1} from ''crossed'' terms of Eq. (14). We have obtained the remarkably larger contribution to the inverse lifetime of this doublet (7.1×10^{10} s^{-1}), which agrees satisfactorily with its measured linewidth, from the second-order terms given in Eq. (13). It should be noted that relaxation processes that involve excitations of localized modes of Γ_{3u} and Γ_{3g} symmetry dominate, yielding more than a half of the total relaxation rate.

VI. CONCLUSION

High-resolution (1–0.005 cm^{-1}) infrared (2000–7000 cm^{-1}) absorption spectra of $CsCdBr_3:Pr^{3+}$ (0.2%) were taken at low temperatures. Crystal-field levels of the $^3H_5$, $^3H_6$, $^3F_2$, and $^3F_3$ multiplets for the symmetric pair center [Pr^{3+}–Cd^{2+} vacancy–Pr^{3+}] were found directly in absorption. The hyperfine structure and inhomogeneous and relaxation-induced widths of several crystal-field levels were measured.

We performed crystal-field calculations in the framework of the semiphenomenological exchange charge model and took into account local lattice deformation around an impurity center. Only two parameters of the model had to be determined by a comparison of calculated and experimental energy levels. The crystal-field parameters so obtained were corrected by fitting the calculated hyperfine structure to the measured one. It follows from our results that despite a large trigonal distortion of the bromine octahedra in the nearest surroundings of impurity Pr^{3+} ions, crystal-field splittings are determined mainly by the cubic component of the crystal field.

Using the results of the crystal-field calculations and of the lattice dynamics analysis we were able to calculate exactly (without any additional fitting parameters) one- and two-phonon spontaneous relaxation rates. The calculated total relaxation rates reveal the linewidths that are in reasonable agreement with the measured ones. The obtained information on the relative efficiency of linear and nonlinear terms in the Hamiltonian of the electron-phonon interaction in stimulation of the phonon emission is important for the thorough derivation of the theory of multiphonon relaxation in rare-earth compounds.

The peculiarities of the electron-phonon interaction effects in $CsCdBr_3:Pr^{3+}$ crystals originate from the specific density of phonon states that extends by only ~ 180 cm^{-1} in the perfect $CsCdBr_3$ lattice, and from the localized modes induced by the impurity dimer centers. Another important feature and, probably, the most interesting result of this study, is a strong suppression of the effective electron-phonon coupling due to a local increase of elastic forces in the activated crystal and the corresponding enhancement of correlations between displacements of the impurity *R* ion and its neighbors.

ACKNOWLEDGMENTS

The encouraging interest of G. N. Zhizhin is acknowledged. This work was supported in part by the RFBR (Grant No. 99–02 16881) and the Russian Ministry of Science (Grant No. 08.02.28 of the Program ''Fundamental Spectroscopy''), and the CNRS-RAS exchange program No. 2631.

[1] F. Ramaz, R.M. Macfarlane, J.C. Vial, J.P. Chaminade, and F. Madeore, J. Lumin. **55**, 173 (1993).
[2] E. Antic-Fidancev, M. Lemaitre-Blase, J.P. Chaminade, and P. Porcher, J. Alloys Compd. **225**, 95 (1995).
[3] K.M. Murdoch and N.J. Cockroft, Phys. Rev. B **54**, 4589 (1996).
[4] J. Neukum, N. Bodenschatz, and J. Heber, Phys. Rev. B **50**, 3536 (1994).
[5] J.P. Chaminade, R.M. Macfarlane, F. Ramaz, and J.C. Vial, J. Lumin. **48&49**, 531 (1991).
[6] J. Heber, M. Lange, M. Altwein, B.Z. Malkin, and M.P. Rodionova, J. Alloys Compd. **275-277**, 181 (1998).
[7] B.Z. Malkin, A.I. Iskhakova, V.F. Tarasov, G.S. Shakurov, J. Heber, and M. Altwein, J. Alloys Compd. **275-277**, 209 (1998).
[8] G.W. Burdick and F.S. Richardson, J. Alloys Compd. **275-277**, 379 (1998).
[9] J.R. Quagliano, N.J. Cockroft, K.E. Gunde, and F.S. Richardson, J. Chem. Phys. **105**, 9812 (1996).
[10] B.Z. Malkin, in *Spectroscopy of Solids Containing Rare-Earth Ions*, edited by A.A. Kaplyanskii and R.M. Macfarlane (North-Holland, Amsterdam, 1987), p.13.
[11] B.Z. Malkin, A.I. Iskhakova, S. Kamba, J. Heber, M. Altwein, and G. Schaack, following paper, Phys. Rev. B.
[12] R.B. Barthem, R. Buisson, F. Madeores, J.C. Vial, and J.P. Chaminade, J. Phys. (France) **48**, 379 (1987).
[13] G. Gorller-Walrand and K. Binnemans, in *Handbook on the Physics and Chemistry of the Rare-Earths*, edited by K.A. Gschneidner and LeRoy Eyring (North-Holland, Amsterdam, 1996), Vol. 23, p. 121.
[14] M.A.H. McCausland and I.S. Mackenzie, Adv. Phys. **28**, 305 (1979).
[15] G. Netz, Z. Phys. B **63**, 343 (1986).
[16] V.C. Das and A.K. Ray Chaudhuri, J. Phys. C **6**, 1385 (1973).
[17] A.J. Freeman and R.E. Watson, Phys. Rev. **127**, 2058 (1962).
[18] E. Clementi and C. Roetti, *Atomic Data and Nuclear Data Tables* (Academic Press, New York, 1974), Vol. 14, Nos. 3–4.
[19] G.L. McPherson, A.M. McPherson, and J.A. Atwood, J. Phys. Chem. Solids **41**, 495 (1980).
[20] L.M. Henling and G.L. McPherson, Phys. Rev. B **16**, 4756 (1977).
[21] V.F. Tarasov, G.S. Shakurov, B.Z. Malkin, A.I. Iskhakova, J. Heber, and M. Altwein, Pis'ma Zh. Éksp. Teor. Fiz. **65**, 535 (1997) [JETP Lett. **65**, 559 (1997)].
[22] M.P. Hehlen and H.U. Gudel, J. Chem. Phys. **98**, 1768 (1993).
[23] E.P. Chukalina, M.N. Popova, E. Antic-Fidancev, and J.P. Chaminade, Phys. Lett. A **258**, 375 (1999).
[24] M.N. Popova, E.P. Chukalina, B.Z. Malkin, and S.K. Saikin, Phys. Rev. B **61**, 7421 (2000).